Experimental and *ab initio* infrared study of χ-, κ- and α-aluminas formed from gibbsite

L. Favaro [a], A. Boumaza [a,b], P. Roy [c], J. Lédion [d], G. Sattonnay [a], J.B. Brubach [c], A.M. Huntz [a], R. Tétot [a,*]

[a] *ICMMO(LEMHE), UMR 8182 CNRS-Université Paris-Sud 11-Orsay, F-91405, France*
[b] *Laboratoire des Structures, Propriétés et Interactions Inter Atomiques (LASPI2A), Centre Universitaire de Khenchela 40000, Algeria*
[c] *Synchrotron SOLEIL, L'Orme des Merisiers, BP 48-Gif-sur-Yvette CEDEX, F-91192, France*
[d] *LIM, UMR CNRS, ENSAM, 151 Bd de l'Hôpital, Paris, F-75013, France*

Keywords:
Gibbsite
Transition alumina
χ-alumina
κ-alumina
α-alumina
Infrared spectroscopy
X-ray diffraction
Ab initio simulations

A B S T R A C T

χ-, κ- and α-alumina phases formed by dehydration of micro-grained gibbsite between 773 and 1573 K are studied using infrared spectroscopy (IR). The structural transitions evidenced by X-ray diffraction (XRD) were interpreted by comparing IR measurements with *ab initio* simulations (except for the χ form whose complexity does not allow a reliable simulation). For each phase, IR spectrum presents specific bands corresponding to transverse optical (TO) modes of Al–O stretching and bending under 900 cm^{-1}. The very complex χ phase, obtained at 773 K, provides a distinctive XRD pattern in contrast with the IR absorbance appearing as a broad structure extending between 200 and 900 cm^{-1} resembling the equivalent spectra for γ-alumina phase. κ-alumina is forming at 1173 K and its rich IR spectrum is in good qualitative agreement with *ab initio* simulations. This complexity reflects the large number of atoms in the κ-alumina unit cell and the wide range of internuclear distances as well as the various coordinances of both Al and O atoms. *Ab initio* simulations suggest that this form of transition alumina demonstrates a strong departure from the simple pattern observed for other transition alumina. At 1573 K, the stable α-Al_2O_3 develops. Its IR spectra extends in a narrower energy range as compared to transition alumina and presents characteristics features similar to model α-Al_2O_3· *Ab initio* calculations show again a very good general agreement with the observed IR spectra for this phase. In addition, for both κ- and α-Al_2O_3, extra modes, measured at high energy (above 790 cm^{-1} for κ and above 650 cm^{-1} for α), can originate from either remnant χ-alumina or from surface modes.

1. Introduction

Applications of alumina are widespread in domains such as protective barriers, catalytic supports, electronic-device fabrication, cutting-tools and surgical materials. This diversity in the applications is due to the fact that Al_2O_3 has the particularity to exist in a variety of metastable structures, the so-called transition alumina (such as χ, κ, γ, δ, θ, η), as well as the stable α-Al_2O_3 phase [1], each having specific physico-chemical and mechanical properties. During high temperature oxidation of aluminum or alumina-forming alloys, before reaching the stable α-Al_2O_3 phase, one or several transition alumina may be formed, depending on the oxidizing atmosphere and the temperature cycle. The first stages of oxidation and the role played by the intermediate steps on the properties of the alumina film is an important task in materials science and is not clearly understood. One of the difficulties rests in the precise characterization of the phases present at a given time, in particular by X-ray diffraction (XRD), which provides similar patterns for various alumina forms [2]. In a previous paper [3], we studied γ-, δ- and θ-transition phases prepared from heat treatment of boehmite, and we showed that combining use of both XRD and infrared spectroscopy (IR) allows characterizing transition alumina formed at different temperatures. In the present paper, the alumina phases (χ-, κ- and α-alumina) synthesized by heating micro grain gibbsite powder have been studied by these two techniques and analysed using *ab initio* calculations. Reaction pathways for the dehydration of gibbsite have been extensively investigated [4–8]. These studies showed that the product depends on the atmosphere and grain size of the starting gibbsite. It is generally accepted that, in air, fine-grained gibbsite is transformed to χ-, κ- or α-alumina, whereas coarse-grained gibbsite, especially in the presence of water vapor, is transformed to boehmite and then to γ-, δ-, θ- or α-alumina, depending on the temperature, as shown in Fig. 1. Following this phase diagram, we prepared four samples at 773, 1173, 1273 and 1573 K from micro-grained gibbsite, expecting synthesize χ-, κ- and α-alumina respectively.

* Corresponding author.
E-mail address: robert.tetot@u-psud.fr (R. Tétot).

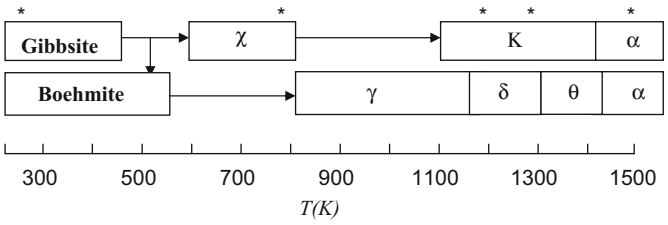

Fig. 1. Sequence of dehydration and transformation of alumina from gibbsite and boehmite [2,5,7,8]. Stars indicate working temperatures.

The paper is structured as follows. In Section 2, experimental (heat treatment, XRD and IR techniques) and *ab initio* techniques are detailed. In Section 3, results obtained on gibbsite, χ-, κ- and α-alumina are presented. We conclude in Section 4.

2. Experimental and modelling techniques

2.1. Experimental

Gibbsite γ-$Al(OH)_3$ micrometric Rectapur powder from Prolabo (98% purity) was used to form metastable χ- and κ-aluminas and stable α-alumina through calcinations at various temperatures (see Fig. 1). The gibbsite powder was calcined in air at temperatures ranging from 773 to 1573 K according to the following heat treatment:

- heating up to the specified temperature at 5 K/min,
- maintaining for 24 h at the calcination temperature,
- cooling down rapidly to room temperature (air quench).

For temperatures lower than 1323 K, the uncertainty on temperature was $\Delta T = \pm 2$ K, while for temperatures above 1373 K, the uncertainty on the temperature was larger, $\Delta T = \pm 10$ K. All the samples were then characterised using both XRD and IR spectroscopy. For IR experiments, 0.01–0.10 mg of the ground powder was mixed with 23 ± 2 mg of CsBr and compressed in a cold 150 MPa isostatic press (CIP) in order to obtain a 200–250 μm thick pellet.

- XRD was performed with a PANalytical X'Pert Pro MRD diffractometer with Cu$K\alpha$ radiation (λ=0.15406 nm). Data were collected with steps of 0.02° (2θ).
- IR spectra were obtained using a Perkin-Elmer spectrometer at 8 cm^{-1} resolution. Fourier transform infrared (FTIR) technique was used in the transmission mode in the 200–4000 cm^{-1} range. For each spectrum, 120 scans were co-added. The transmission spectra were obtained by dividing the signal transmitted through the pellet (I) by the signal measured through an aperture of the same dimensions (I_0). All IR spectra are presented in absorbance ($A = -ln(I/I_0)$) as a function of the incident wavenumbers ω. The apparatus was purged by dry nitrogen to minimize absorption by water vapor and CO_2 gas.

2.2. Ab initio modelling

The equilibrium structural parameters and Γ-point vibrational frequencies of α- and κ-Al_2O_3 bulk have been calculated using the periodic *ab initio* program Crystal 06 [9], which adopts an all-electron Gaussian-type basis set. The calculations have been performed at the DFT level using the B3LYP functional, based on the Vosko–Wilk–Nusair correlation potential [10] and the Becke's 3 parameters functional for exchange energy [11]. The 85–11G(*) basis set for aluminum [12] and the 88–31G(*) basis set for oxygen [13] were used. The shrinking factors were set to 4 4 4, corresponding to 30 K-points in the irreducible Brillouin zone. The integration grid was set by the keyword "XLGRID", defining a pruned grid composed of 75 radial points and 974 angular points. The vibrational spectra were computed after a full structural optimization as described by Pascale et al. [14]. The convergence criteria for optimization steps were, on one side, 0.00003 for the maximum component of displacement and 0.00012 for the maximum mean root square of the forces and, on another side, 10^{-10} Hartree as SCF energy convergence criterion. These tight convergence choices ensured the vibrational spectrum to be calculated with a precision of approximately 10 cm^{-1}. The precision on intensities should be within a factor of 2. For the study of transmission through samples, only the transverse optical modes are compared with measurements. Extra details on the calculation of vibrational frequencies of crystalline compounds with Crystal code can be found in Refs. [9,14,15].

3. Results

3.1. Gibbsite

Gibbsite (γ-$Al(OH)_3$) has monoclinic symmetry (a=8.684, b=5.078, c=9.736 Å, β=94,54°) with the space group $P2_1/n$, and the unit cell contains eight $Al(OH)_3$ units [16]. Gibbsite is characterized by the stacking of two-layer units (AA or BB) of hydroxyl sheets with the sequence ABBAABBA… where hydroxyl sheets of the adjacent Gibbsite layers face the c direction [17]. In Fig. 2a, the XRD pattern obtained on the as received gibbsite powder shows a good agreement with the reference XRD pattern (33-0018 JCPDS file). The IR spectrum obtained for the same sample is presented Fig. 2b. In the high energy range, four strong absorption bands (3397, 3467, 3529 and 3623 cm^{-1}) are in very good agreement with the experimental and theoretical spectra by Balan et al. [18] and Kloprogge et al. [5, 6] in the range of the OH-stretching bands of gibbsite. At lower energy, bands extending in the 250–1000 cm^{-1} range may be attributed first to the bending and then to the stretching of Al–O bonds, while the strong band at 1020 cm^{-1} probably results from hydroxyl deformation [5].

3.2. Phase transitions induced by heat treatment of gibbsite

When heating up fine-grained gibbsite, most OH groups are eliminated, and various forms of alumina are formed with the sequence: gibbsite $\rightarrow$χ-$\rightarrow$κ-$\rightarrow$α-Al_2O_3 when temperature increases. In order to study these phases, we performed XRD and IR measurements on four samples prepared from gibbsite calcined for 24 h at 773, 1173, 1273 and 1573 K respectively.

According to Fig. 1, at 773 K, the χ phase is expected. In spite of many investigations since the 1950's [4, 17, 19–21], the crystal structure of χ-alumina is still uncertain. Stumpth et al. [19] assumed a cubic (not spinel) unit cell of lattice parameter a=7.95 Å (04-0880 JCPDS file). On the other hand, two hexagonal structures have been suggested, either with the parameters a=5.56 Å and c=13.44 Å [21] or with a=5.57 Å and c=8.64 Å [20] (13-0373 JCPDS file). The two previous hexagonal unit cells may be described respectively as a stacking of 6 and 4 close-packed oxygen layers, of approximately the same thickness (2.24 and 2.16 Å) as the Al–OH layers in gibbsite (2.12 Å). More recently, Kogure [17] proposed a hexagonal lattice with a=4.9 Å and an undefined c length indicating that χ-alumina structure can be regarded as random close packing of gibbsite-like

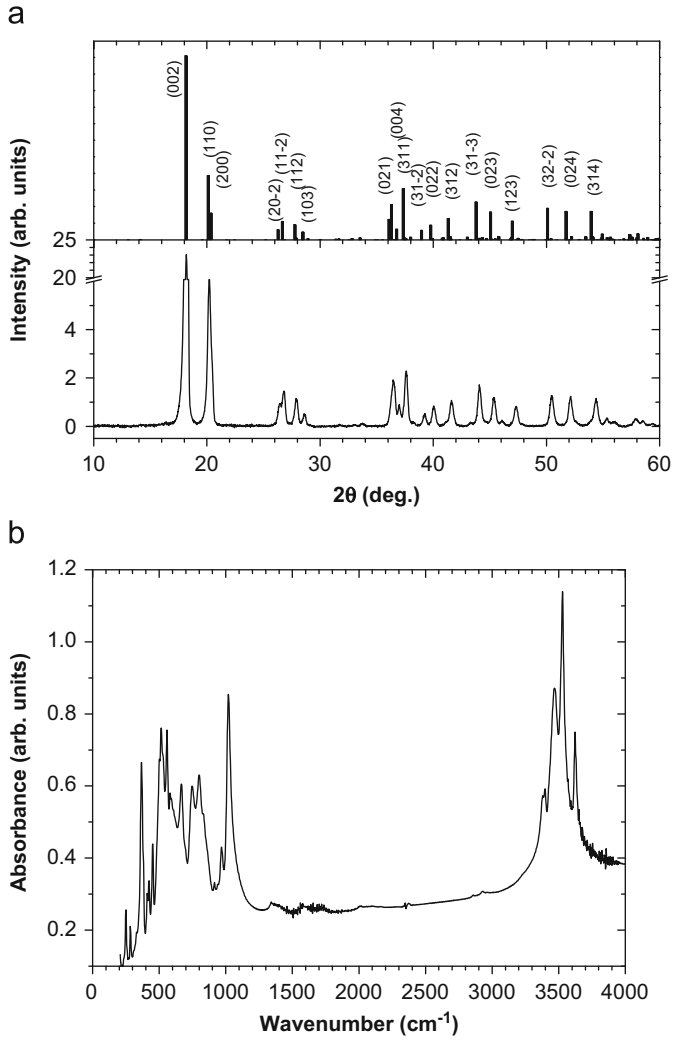

Fig. 2. Gibbsite: (a) XRD measured and from 33-0018 JCPDS file, (b) IR absorbance spectrum.

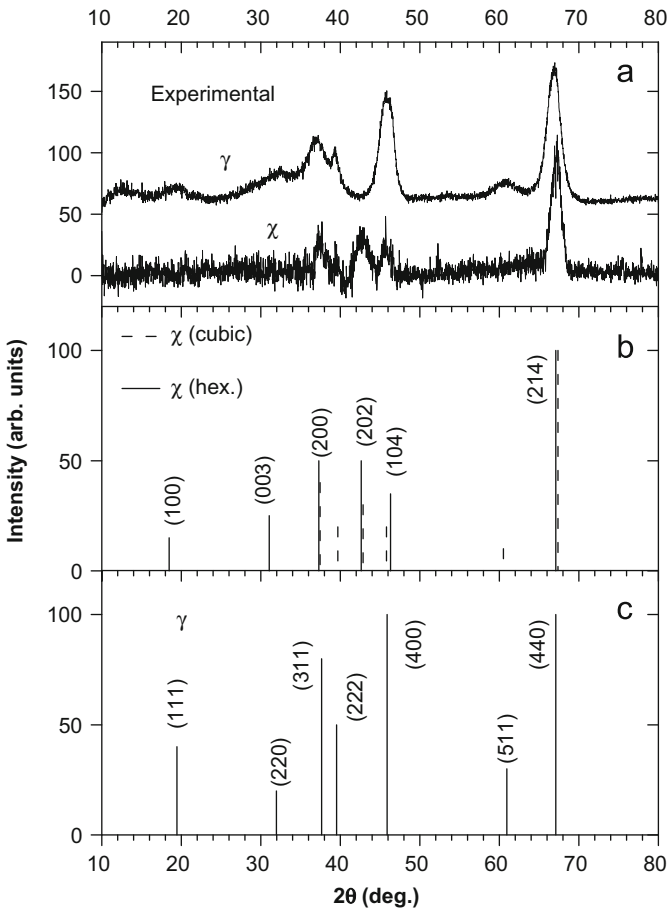

Fig. 3. XRD patterns: (a) alumina formed from gibbsite calcined for 24 h at 773 K (expected χ phase) and γ-alumina formed from boehmite [18], (b) χ-aluminas from cubic JCPDS 04-0880 file and hexagonal JCPDS 13-0373 file (the assignment refers to the hexagonal structure), (c) γ-alumina from JCPDS 10-0425 file.

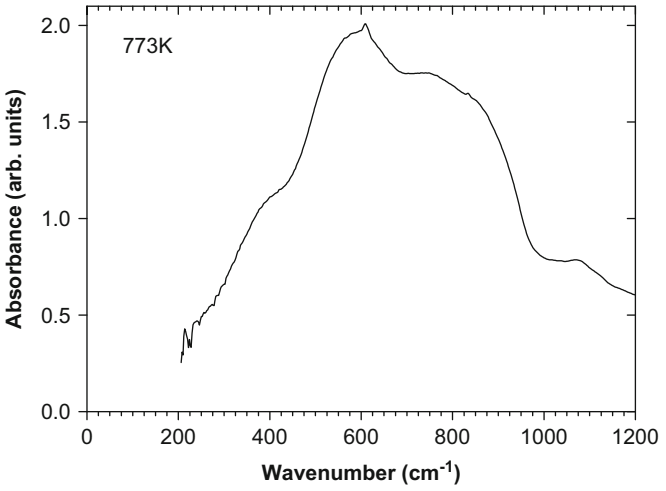

Fig. 4. IR absorbance spectrum of alumina formed from gibbsite calcined for 24 h at 773 K.

layers. The XRD pattern of 773 K sample is shown Fig. 3a together with the γ pattern from [3] and is compared with the two reference patterns (04-0880 JCPDS and 13-0373 JCPDS files) corresponding to the cubic and hexagonal χ structures respectively (Fig. 3b). Moreover, according to Fig. 1, in particular experimental conditions, heating gibbsite may also result in the formation of γ phase via the transition gibbsite→boehmite [4, 7]. To check this pathway, the reference XRD pattern (10-0425 JCPDS file) of γ-alumina is reported Fig. 3c. The comparison of experimental γ and χ-Al_2O_3 XRD patterns (Fig. 3a), and in particular the band (202) at 2θ=43°, present in χ reference pattern (Fig. 3b) and not observed in γ reference pattern (Fig. 3c), allows an unambiguous assignment to the χ phase for the 773 K sample. Fig. 3a also shows that χ sample is poorly crystallized as suggested by the width of the peaks, most likely due to the intrinsic disordered character of the χ phase. As a consequence, it is somewhat risky to choose between the cubic and the hexagonal form, in spite of the presence of a small peak at 2θ=40° which can suggest the cubic phase. IR absorption has been measured on the same 773 K sample and is presented in Fig. 4. It appears as a wide unresolved pattern extending from 350 to 850 cm^{-1} with maximum absorbance around 410, 600 and 800 cm^{-1}. This spectrum resembles closely the γ-Al_2O_3 phase [3] and, as such, seems characteristic of a complex and disordered crystallographic structure. However, in this case, the broad band around 800 cm^{-1} contains two substructures centered on around 750 and 830 cm^{-1}. It should be pointed out that the present χ-alumina contains small amounts of hydroxyl ions as demonstrated by the presence of a band around 1080 cm^{-1} characteristics of a bending mode [5]. The similarities with the γ phase absorbance spectrum suggests that the lowest energy broad bands (around 400 cm^{-1}) can be assigned to Al–O bending modes,

while the two higher energy structures (600 and 800 cm^{-1}) are dominated by stretching Al–O modes for the AlO_6 octahedron and AlO_4 tetrahedron respectively [3]. The band positions are presented in Table 1 (first column).

For samples prepared at 1173, and 1273 K, the κ phase is expected (see Fig. 1). Contrary to the χ phase, the crystal structure of κ-alumina is well known (see for example Ref. [22] and references therein). κ-alumina is orthorhombic with the space group $pna2_1$ and results in ten independent atoms positions (four Al and six O). In Table 2 are displayed the main characteristic of the κ phase: atomic parameters, distances of Al–O bonds and coordinances of atoms. Among the four Al, three are six-coordinated (AlO_6 octahedra) and one is four-coordinated (AlO_4 tetrahedra). Among the three AlO_6 octahedra, two of them present one particularly long Al–O bond (2.27 Å for Al_2, 2.15 Å for Al_4) with respect to the five other bonds. In the following, these two AlO_6 units will be noted as AlO_6 (5+1) (see Table 2). Concerning oxygen atoms, two are four-coordinated, three are three-coordinated, and one is five-coordinated, which is specific of this phase. The experimental XRD patterns measured on the 1173 and 1273 K samples and compared with the calculated reference pattern of κ-alumina are shown in Fig. 5a–c. The experimental XRD pattern at 1173 K is specific of a pure κ-alumina (Fig. 5a), in contrast with the 1273 K sample in which some minor bands, noted in Fig. 5b, indicate the presence of a small quantity of α-alumina. Nevertheless, the presence of remnant χ-phase cannot be excluded as all the χ peaks also appear in κ structure. Note that the experimental XRD patterns show well crystallized phases, in contrast with the χ phase. As a consequence of the great variety of crystallographic sites, the infrared spectrum is expected to be complex. Indeed, the infrared absorbance spectra for 1173 and 1273 K samples (Figs. 6a) show a large number of well resolved bands in a wide energy range extending from 200 to 900 cm^{-1}. In order to analyse these spectra, we have calculated the infrared transverse optical modes using *ab initio* methods described before. These bands are represented Fig. 6b. as sticks whose length is proportional to their oscillator strength. To help the comparison with experiment it is also represented as a sum of 20 cm^{-1} width Gaussians.

As a preliminary step we have separated the calculated absorption range in six regions, according to their dominant contributions reported in Table 1, second column. Accordingly, in the discussion, we report for each energy region, the calculation main findings and use them as a guide for attributing the equivalent region in the experimental spectra.

I. The lowest energy region ($\omega \leq 200\,cm^{-1}$) is dominated by contributions from Al–O stretching modes involving five-coordinated oxygen (OV) and Al (5+1), the two main ones calculated at 147 and 180 cm^{-1}. This unusual low energy for a Al–O stretching mode may be the signature of the loosely bound Al–O with very large interatomic distances (2.15 and 2.27 Å, see Table 2) determined for OV. This region is not covered by our experimental measurements limited to $\omega \geq 200\,cm^{-1}$ and is not reported in Table 1.

II. The second energy region (from 200 to 440 cm^{-1}) is dominated by Al–O bending as for other forms of alumina ([3] and references therein). However in this case, the Al–O pairs largely belong to AlO_6 octahedra, the Al–O bending for AlO_4 tetrahedra contributing only to small bands. Nevertheless, the two smaller contributions calculated at 209 and 236 cm^{-1}, attributed to Al–O bending mode for AlO_6 octahedra and AlO_4 tetrahedra

Table 1
Experimental (Exp) band positions (cm^{-1}) for alumina formed from gibbsite calcined for 24 h at 773 K (χ-Al_2O_3), 1273 K (κ-Al_2O_3) and 1573 K (α-Al_2O_3), together with assignments from *ab initio* calculations for κ-and α-Al_2O_3 ($B \equiv$ Al–O bending, $S \equiv$ Al–O stretching).

Chi	**Kappa**		**Alpha**	
Exp.	Exp.	Assignment (*ab initio* calc.)	Exp.	Assignment (*ab initio* calc.)
	240	**Region II**		
	270	(200–440)		
	300			
	335	AlO_6 (B)		
	372	+	386	
	407	AlO_4 (B)		AlO_6 (B)
~410	422			
	455		449	
	487	**Region III**	**484**	**Surface mode?**
	506	(440–630)		
	536			
	563	AlO_6 (S+B)		
~590	597	+	594	
~610	630	AlO_4 (S+B)		AlO_6 (S)
	641		640	
	657			
	690	**Region IV**		
	710	(630–750)		
~750	737	AlO_6 (S)		
	782	**Region V**		
		(630–750)	**650–800**	**Surface modes or water**
		AlO_4 (S)		
	819	**Region VI**		
~830	838	(790–930)		
		Mixed contribution		
	~**880**	**Surface modes ?**		
~1080	**1070**	**Al–O–H groups (B)**	1070	Al–O–H groups (B)

Energy regions II, III, IV, V and VI are defined in Fig. 6.

Table 2
Atomic parameters and interatomic distances in κ-Al_2O_3.

Atomic parameters for κ-Al_2O_3	(Space group: $Pna2_1$)		
a=4.8437 Å b=8.3300 Å c=8.9547 Å a/b=0.5815 b/c=0.9302 c/a=1.8487 V=361.30 Å^3			
Atom	x/a	y/b	z/c
Al1	0.679	0.842	0.000
Al2	0.185	0.343	0.787
Al3	0.812	0.649	0.697
Al4	0.668	0.470	0.999
O1	0.329	0.831	0.893
O2	0.025	0.491	0.629
O3	0.472	0.665	0.638
O4	0.515	0.673	0.121
O5	0.861	0.330	0.866
O6	0.336	0.499	0.900
Distances			
Atom1	Atom2	d_{12}(Å)	Unit
Al1	O6	1.770	AlO_6
	O1	1.877	
	O4	1.947	
	O1	1.950	
	O4	1.959	
	O2	1.963	
Al2	O5	1.725	AlO_6 (5+1)
	O6	1.802	
	O5	1.818	
	O2	2.030	
	O4	2.083	
	O4	2.270	
Al3	O3	1.735	AlO_4
	O1	1.765	
	O2	1.780	
	O3	1.811	
Al4	O3	1.809	AlO_6 (5+1)
	O6	1.852	
	O5	1.911	
	O2	1.916	
	O1	2.063	
	O4	2.145	
O1	Al3	1.765	OIV
	Al1	1.877	
	Al1	1.950	
	Al4	2.063	
O2	Al3	1.780	OIV
	Al4	1.916	
	Al1	1.963	
	Al2	2.030	
O3	Al3	1.735	OIII
	Al4	1.809	
	Al3	1.811	
O4	Al1	1.946	OV
	Al1	1.959	
	Al2	2.083	
	Al4	2.145	
	Al2	2.270	
O5	Al2	1.725	OIII
	Al2	1.818	
	Al4	1.911	
O6	Al1	1.770	OIII
	Al2	1.802	
	Al4	1.852	

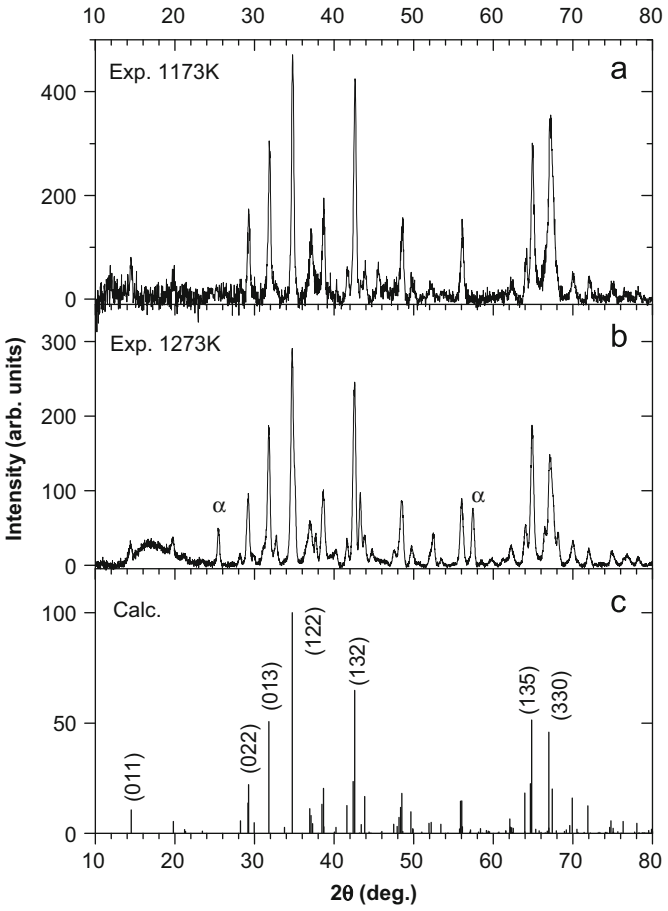

Fig. 5. XRD patterns: (a) alumina formed from gibbsite calcined for 24 h at 1173 K (expected κ phase), (b) alumina formed from gibbsite calcined for 24 h at 1273 K, (c) reference calculated pattern of κ-alumina described in Table 2.

respectively, may correspond to the two small experimental peaks at 240 and 270 cm^{-1} (see Table 1). It seems that this energy region may be compared with the experimental energy range between 200 and 460 cm^{-1} (first measured area in Fig. 6a). Indeed, as predicted by calculations, the oscillator strength raises as the energy increases.

III. The next theoretical energy region (from 440 to 630 cm^{-1}) is characterized by the highest intensity bands both experimentally and theoretically with all calculated bands resulting from mixed contributions from Al–O bending and stretching motions for both AlO_4 and AlO_6. The four main calculated structures as well as their attributions are as follows:

- the band at 483 cm^{-1} is a mixed contribution of Al–O stretching between AlO_6 (5+1) and AlO_4. Although this assignment is coherent with the previous observation of Al–O stretching for AlO_6 for the other alumina, the energy is somewhat low for Al–O stretching mode for AlO_4 [3].
- the band at 564 cm^{-1} results from two unresolved structures at 562 and 565 cm^{-1}. The first one can be assigned to Al–O bending for AlO_6 (5+1), while the second is a pure Al–O stretching mode for AlO_4. Again this energy seems low for this assignment by analogy with other alumina phases.
- the band at 593 cm^{-1} is a mixed contribution of Al–O stretching and bending for AlO_6 (5+1).
- the intense band at 621 cm^{-1} involves stretching and bending of all coordinance Al and O atoms.

Experimentally, the energy range between 480 and 670 cm^{-1}, dominated by seven bands (see Fig. 6a and Table 1) resembles

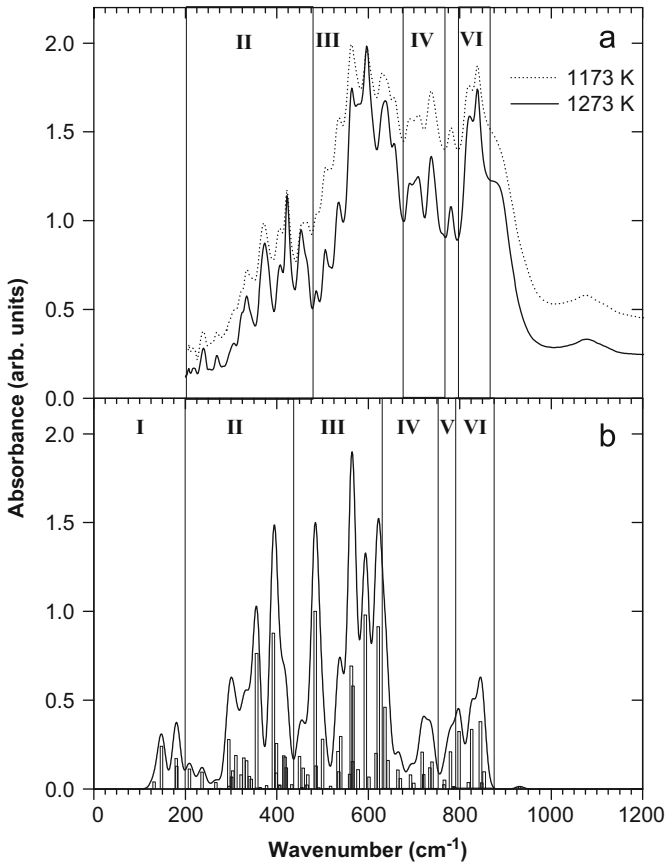

Fig. 6. IR absorbance spectra: (a) alumina formed from gibbsite calcined for 24 h at 1173 K (expected κ phase) and 1273 K, (b) calculated spectrum of κ-alumina: sticks are proportional to oscillator strength (maximum intensity normalized at 1) and line represents a sum of 20 cm^{-1} width Gaussians (maximum intensity normalized at 2). The energy range is separated in six regions.

the theoretical range III as described previously. In particular the four last peaks at 563, 597, 641 and 657 cm^{-1} may correspond to the calculated 562, 565, 593 and 620 cm^{-1} structures. In contrast, the 480–540 cm^{-1} range shows three medium intensity bands at 487, 506 and 536 cm^{-1} unlike the theoretical predictions presenting one dominating band (483 cm^{-1}) accompanied by smaller structures.

IV. The fourth energy region expands theoretically from 630 to 750 cm^{-1}. It is clearly dominated by Al–O stretching for AlO_6, in good agreement with other alumina structures, and some smaller contributions from other modes. More precisely, four main bands are calculated at 635, 665, 718 and 736 cm^{-1}. The first one appears as a shoulder on the last intense peak of the previous energy region and may correspond, on the experimental spectra, to the unresolved structure at 657 cm^{-1} (see Table 1). The next three bands may be consistent with the 690, 710 and 737 cm^{-1} measured ones.

V. The next region includes three modes of Al–O stretching for AlO_4, the dominating one being at 778 cm^{-1} which may match with the experimental structure at 782 cm^{-1}.

VI. The last region extending above 790 cm^{-1} contains again multiple contributions with maximum oscillator strength around 835cm^{-1}. Experimentally, in this region, two bands at 819 and 838 cm^{-1} superimposed on a wide and intense background peaking at 880 cm^{-1} are observed. This intense continuum is not predicted theoretically for the κ structure. Two assignments may be suggested. First, a remnant of the χ structure (see Fig. 4) for which the absorbance range extends up to 900 cm^{-1}. Alternatively, surface modes, not included in the simulations, may give rise to higher energy bands. Notice that the presence of these modes may be allowed by the microgranular nature of our samples.

Finally, a small quantity of OH from the initial gibbsite is still present as attested by the presence of small bands assigned to hydroxyl deformation around 1070 cm^{-1}.

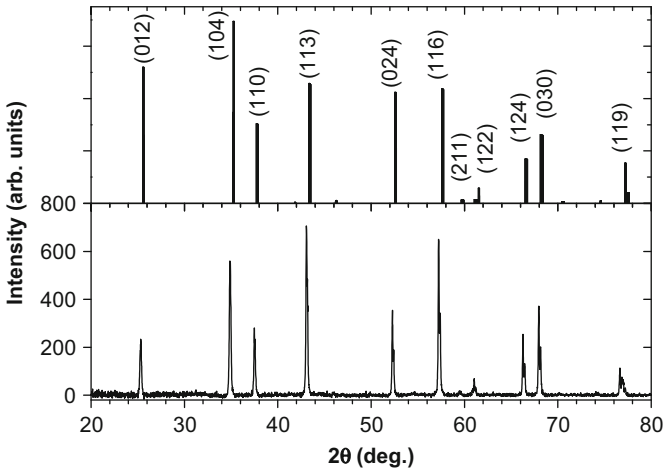

Fig. 7. XRD pattern of alumina formed from gibbsite calcined for 24 h at 1573 K (expected α phase) (lower part) and pattern from 42-1468 JCPDS file (upper part).

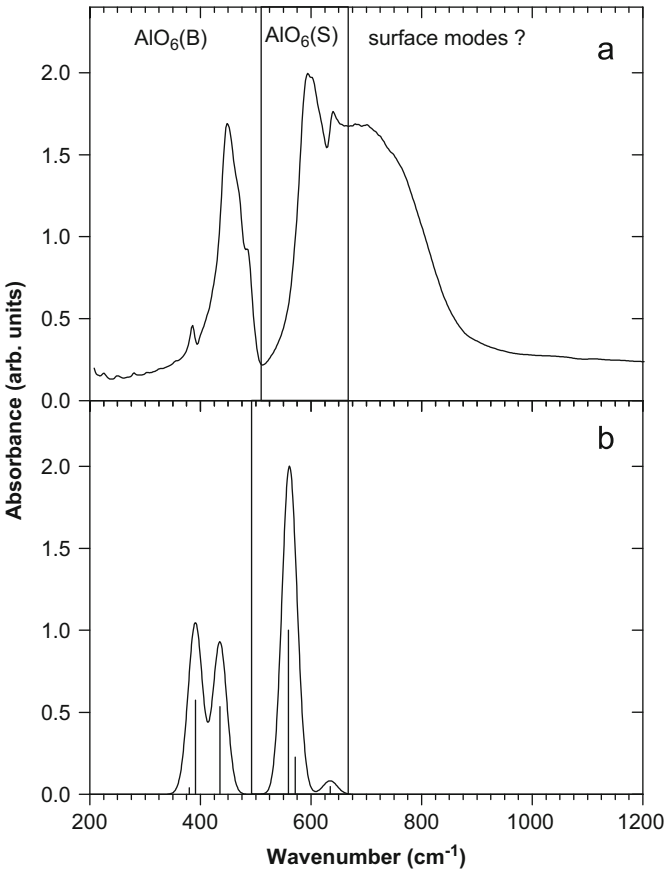

Fig. 8. IR absorbance spectra: (a) alumina formed from gibbsite calcined for 24 h at 1573 K (expected α phase), (b) calculated spectrum of α-alumina: sticks proportional to oscillator strength (maximum intensity normalized at 1), line represents a sum of 30 cm^{-1} width Gaussians (maximum intensity normalized at 2).

3.3. Alpha alumina (corundum)

When heating up at temperature above 1573 K for 24 h, gibbsite transforms into α-alumina, the stable structure (Fig. 1). The XRD pattern of the 1573 K sample (Fig. 7) shows that only α-Al_2O_3 is present when compared with 42–1468 JCPDS file. In this structure, tetrahedral Al^{3+} ions are no longer present and only AlO_6 octahedron remain. Accordingly, the measured IR spectra corresponding to this temperature (Fig. 8a) shows a simple spectrum as was observed in previous works [23, 3], with four main structures visible between 350 and 650 cm^{-1}. The lowest energy peaks (under 500 cm^{-1}) are assigned to Al–O bending for AlO_6, the bands above 500 cm^{-1} resulting from Al–O stretching (see Table 1, third column). The comparison with equivalent spectrum simulation (Fig. 8b) shows that the main bands are well predicted confirming indeed the assignment above. Nevertheless, some discrepancies can be noticed. Firstly, a shoulder at 484 cm^{-1} is present on the higher energy side of the bending mode at 449 cm^{-1} on the experimental spectrum. More importantly, a wide and intense continuum dominates the 650–800 cm^{-1} region where no structures are predicted by our calculations. This high energy structure clearly resembles the high energy continuum already observed on the κ spectrum. In analogy with the suggestion made for the latter case, we suggest these extra structures to result from either surface modes, residual water or remnant transition phase modes, although no transition alumina is detected from the XRD. Notice that one can also exclude contributions from longitudinal optical (LO) modes as these are calculated around 900 cm^{-1}.

4. Conclusions

The aim of this work was to study the alumina phase resulting from thermal treatment of gibbsite. The combined use of both XRD and IR spectroscopy together with *ab initio* simulations allowed studying the sequence: gibbsite →χ-→κ-→α-Al_2O_3 with increasing temperature from 773 to 1573 K. No transition from gibbsite to boehmite together with the subsequent transition boehmite →γ-→δ-→θ-→α-Al_2O_3 was observed. The evolution gibbsite →α-Al_2O_3 is resumed in Fig. 9(a and b) presenting the XRD patterns and IR spectra along the sequence. Both techniques show that heating gibbsite, a very well crystallized solid, at 773, 1173 and 1573 K, yields respectively the semi-amorphized χ phase, followed by the complex but well crystallized κ phase and finally the simple and highly crystallized stable α-Al_2O_3.

At 773 K, infrared spectra shows a wide structure with three broad unresolved bands extending between 200 and 900 cm^{-1} in close resemblance with the equivalent spectra of γ phase [3]. In contrast, the XRD measurements allow distinguishing these two transition alumina. The absence of a reliable crystallographic structure for the χ-alumina prevents *ab initio* calculations and only experimental results are available.

As shown by XRD analysis, at 1173 K, κ-alumina is formed. *Ab initio* calculations predict a very complex IR spectrum with a large number of bands extending between 130 and 930 cm^{-1}, in good qualitative agreement with the measured spectra. This complexity reflects the large number of different crystallographic non equivalent atoms (four Al and six O) accompanied by the wide range of internuclear distances (extending from 1.72 to 2.27 Å) and also the various coordinance (AlO_6, AlO_6 (5+1), AlO_4, OIII, OIV and OV). Notice that this last oxygen coordinance (OV) is specific for κ- transition alumina and gives rise to the low energy bands calculated under 200 cm^{-1}. Another consequence of this complexity is the departure from the simple band energy sequence: Al–O bending for AlO_4, Al–O bending for AlO_6, Al–O stretching for AlO_6 and Al–O stretching for AlO_4, as was evidenced for other forms of alumina [3, 24] and references therein. Nevertheless, from the *ab initio* calculations, six energy regions have been distinguished according to their main

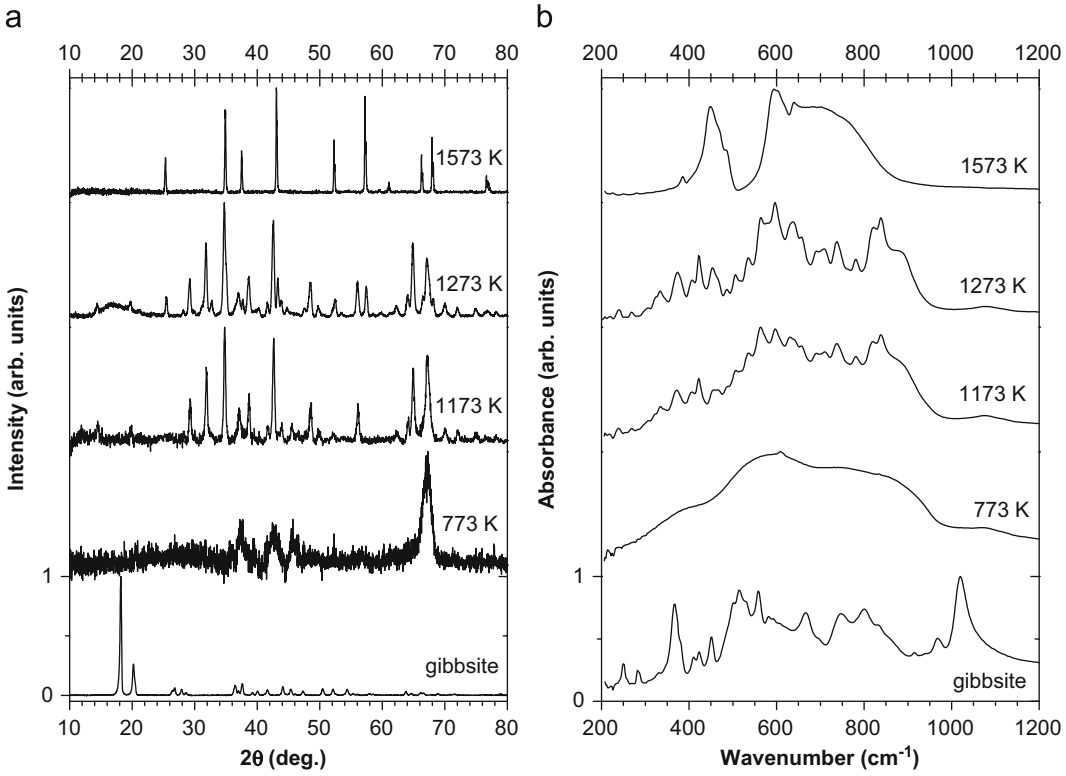

Fig. 9. XRD patterns (a) and IR absorbance spectra (b) for gibbsite and for alumina formed from gibbsite calcined for 24 h at 773, 1173, 1273 and 1573 K. All intensity maxima are normalized at 1.

features and a tentative assignment was suggested, based on similarities between theoretical and experimental spectra.

When heating gibbsite at 1573 K, as expected, the stable α-alumina forms. For this phase, a good agreement is observed between experimental and simulated IR spectra.

For both κ and α phases, extra modes unpredicted by *ab initio* calculations are observed experimentally. They can be explained by either remnant χ transition alumina or surface modes. A specific study on these surface modes is in progress [25].

The precise characterization made in this paper and in the previous one [3] may constitute a basis for investigations on thin layers of alumina form under various experimental conditions on alumina-forming materials [25].

Acknowledgments

We wish to thank Celine Byl and Michaele Herbst (ICMMO (LEMHE)) for technical support and Ross Gash and Laurent Manceron for a critical reading of the manuscript. We also thank the Division des Ressources Informatiques (DRI) of SOLEIL and the Direction Informatique (DI), Orsay, for providing computational resources.

References

[1] I. Levin, D.G. Brandon, J. Am. Ceram. Soc. 81 (1998) 1995.
[2] S. Chevalier, R. Molins, O. Heintz, J.P. Larpin, Mater. High Temp. 3–4 (2005) 365.
[3] A. Boumaza, L. Favaro, J. Lédion, G. Sattonnay, J.B. Brubach, P. Berthet, A.M. Huntz, P. Roy, R. Tétot, J. Solid State Chem. 182 (2009) 1171.
[4] B. Whittington, D. Ilievski, Chem. Eng. J. 98 (2004) 89.
[5] J.T. Kloprogge, H.D. Ruan, R.L. Frost, J. Mater. Sci. 37 (2002) 1121.
[6] R.L. Frost, J.T. Kloprogge, S.C. Russel, J.L. Szetu, Appl. Spectrom. 53 (1999) 423.
[7] K. Wefers, C. Misra, Alcoa Technical Paper No. 19 (1987) (revised).
[8] J. Rouquerol, F. Rouquerol, M. Ganteaume, J. Catal. 36 (1975) 99.
[9] R. Dovesi, V.R. Saunders, C. Roetti, R. Orlando, C.M. Zicovich-Wilson, F. Pascale, B. Civalleri, K. Doll, N.M. Harrison, I.J. Bush, Ph. D'arco, M. Llunell, Crystal 06 User's Manual, 2006, University of Torino, Torino.
[10] S.H. Vosko, L. Wilk, M. Nusair, Can. J. Phys. 581 (1980) 200.
[11] A.D. Becke, J. Chem. Phys. 98 (1993) 5648.
[12] M. Catti, G. Valerio, R. Dovesi, M. Causa', Phys. Rev. B 49 (1994) 14179.
[13] B. Civalleri, P. Ugliengo, J. Phys. Chem. 104 (2000) 9419.
[14] F. Pascale, C.M. Zicovich-Wilson, F. Lopez Gejo, B. Civalleri, R. Orlando, R.J. Dovesi, Comput. Chem. 25 (2004) 888.
[15] B. Montanari, B. Civalleri, C.M. Zicovich-Wilson, R. Dovesi, Int. J. Quantum Chem. 106 (2006) 1703.
[16] H. Saalfeld, M. Wedde, Zeitschrift für Kristallographie 139 (1974) 129.
[17] T. Kogure, J. Am. Ceram. Soc. 82 (1999) 716.
[18] E. Balan, M. Lazzeri, G. Morin, F. Mauri, Am. Mineral. 91 (2006) 115.
[19] H.C. Stumpf, A.S. Russel, J.W. Newsome, C.M. Tucker, Ind. Eng. Chem. 42 (1950) 1398.
[20] G.W. Brindley, J.O. Choe, Am. Mineral. 46 (1961) 771.
[21] H.N. Saalfeld, Jb. Miner. Abh. 95 (1960) 1–87.
[22] B. Ollivier, R. Retoux, P. Lacorre, D. Massiot, G. Férey, J. Mater. Chem. 7 (1997) 1049.
[23] P. Tarte, Spectrochem. Acta 23A (1967) 2127.
[24] P. Colomban, J. Mater. Sci. 24 (1989) 3002.
[25] L. Favaro, P. Roy, E. Amzallag, R. Tétot, in preparation.